JOURNAL OF GEOPHYSICAL RESEARCH, VOL. 114, D12302, doi:10.1029/2008JD011297, 2009



# Eddy covariance observations of surface leakage during shallow subsurface $CO_2$ releases

Jennifer L. Lewicki,[1] George E. Hilley,[2] Marc L. Fischer,[3] Lehua Pan,[1] Curtis M. Oldenburg,[1] Laura Dobeck,[4] and Lee Spangler[4]

Received 15 October 2008; revised 19 February 2009; accepted 20 April 2009; published 18 June 2009.

[1] We tested the ability of eddy covariance (EC) to detect, locate, and quantify surface $CO_2$ flux leakage signals within a background ecosystem. For 10 days starting on 9 July 2007, and for 7 days starting on 3 August 2007, 0.1 (Release 1) and 0.3 (Release 2) t $CO_2$ $d^{-1}$, respectively, were released from a horizontal well ~100 m in length and ~2.5 m in depth located in an agricultural field in Bozeman, Montana. An EC station measured net $CO_2$ flux ($F_c$) from 8 June 2006 to 4 September 2006 (mean and standard deviation = −12.4 and 28.1 g $m^{-2}$ $d^{-1}$, respectively) and from 28 May 2007 to 4 September 2007 (mean and standard deviation = −12.0 and 28.1 g $m^{-2}$ $d^{-1}$, respectively). The Release 2 leakage signal was visible in the $F_c$ time series, whereas the Release 1 signal was difficult to detect within variability of ecosystem fluxes. To improve detection ability, we calculated residual fluxes ($F_{cr}$) by subtracting fluxes corresponding to a model for net ecosystem exchange from $F_c$. $F_{cr}$ had reduced variability and lacked the negative bias seen in corresponding $F_c$ distributions. Plotting the upper 90th percentile $F_{cr}$ versus time enhanced the Release 2 leakage signal. However, values measured during Release 1 fell within the variability assumed to be related to unmodeled natural processes. $F_{cr}$ measurements and corresponding footprint functions were inverted using a least squares approach to infer the spatial distribution of surface $CO_2$ fluxes during Release 2. When combined with flux source area evaluation, inversion results roughly located the $CO_2$ leak, while resolution was insufficient to quantify leakage rate.

**Citation:** Lewicki, J. L., G. E. Hilley, M. L. Fischer, L. Pan, C. M. Oldenburg, L. Dobeck, and L. Spangler (2009), Eddy covariance observations of surface leakage during shallow subsurface $CO_2$ releases, *J. Geophys. Res.*, *114*, D12302, doi:10.1029/2008JD011297.

## 1. Introduction

[2] One approach being considered to help mitigate rising atmospheric $CO_2$ concentrations is geologic carbon sequestration (GCS) [e.g., *International Energy Agency*, 1997, 2004; *Intergovernmental Panel on Climate Change*, 2005]. The possibility of leakage of $CO_2$ from underground storage sites along permeable pathways such as well bores or faults is a primary concern for the safety and effectiveness of GCS. Should it occur, this leakage could have harmful effects on the near-surface environment. Therefore, in addition to $CO_2$ capture, transportation, and injection technology, GCS requires monitoring approaches with the ability to detect, locate, and quantify potential $CO_2$ leakage in the near-surface environment.

[3] While numerous techniques are available to measure $CO_2$ concentrations and fluxes within the near-surface environment, detection and characterization of potential $CO_2$ leakage from geologic storage reservoirs will pose a challenge owing to the large spatial and temporal variation in background $CO_2$ fluxes [e.g., *Lewicki et al.*, 2005; *Cortis et al.*, 2008]. Eddy covariance (EC) is a micrometeorological approach traditionally used to measure trace gas and heat fluxes across the interface between the atmosphere and a plant canopy under certain atmospheric and terrain conditions [e.g., *Baldocchi*, 2003]. EC offers the benefit of an automated flux measurement that does not interfere with the ground surface and is averaged over both time and space, with the spatial scale significantly larger ($m^2$–$km^2$) than that of many other ground-based techniques. For these reasons, EC has been proposed for use in GCS monitoring programs [e.g., *Oldenburg et al.*, 2003; *Miles et al.*, 2005; *Leuning et al.*, 2008; S. M. Benson, Monitoring carbon dioxide sequestration in deep geological formations for inventory verification and carbon credits, paper presented at *SPE Annual Technical Conference*, Society of Petroleum Engineers, San Antonio, Texas, 2006]. Several studies have used EC

[1]Earth Sciences Division, Lawrence Berkeley National Laboratory, Berkeley, California, USA.
[2]Department of Geological and Environmental Sciences, Stanford University, Stanford, California, USA.
[3]Environmental Energy Technology Division, Lawrence Berkeley National Laboratory, Berkeley, California, USA.
[4]Department of Chemistry and Biochemistry, Montana State University, Bozeman, Montana, USA.


0148-0227/09/2008JD011297$09.00

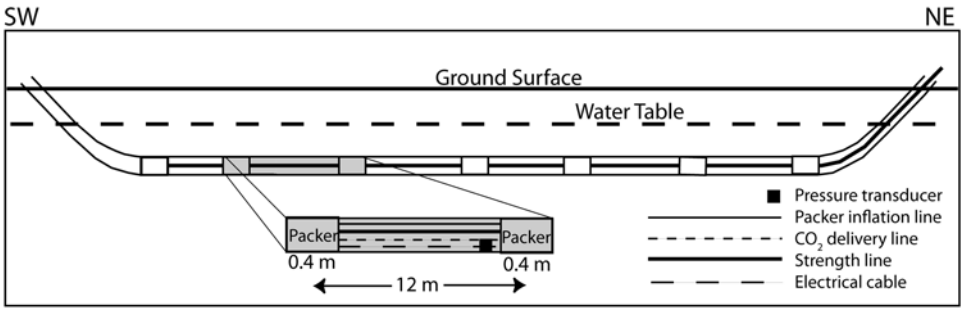


**Figure 1.** Schematic of the $CO_2$ release well at Montana State University. Gray zone is expanded to show example of an ~12-m perforated well zone from which $CO_2$ was released, bounded by two ~0.4-m inflatable packers.

to measure artificial tracers released at the surface in simple geometric configurations to verify footprint models [e.g., *Foken and Leclerc*, 2004, and references therein]. EC has also been shown to provide reliable measurements of relatively large-magnitude volcanic $CO_2$ fluxes resulting from gas migration from natural geologic reservoirs to the surface [*Anderson and Farrar*, 2001; *Werner et al.*, 2000, 2003; *Lewicki et al.*, 2008]. However, the ability of EC to detect, locate, and quantify potentially small subsurface-derived $CO_2$ leakage signals within the large background variability of ecological fluxes is largely untested.

[4] A facility was recently built in an agricultural field at Montana State University by the Zero Emissions Research and Technology (ZERT) Project, where $CO_2$ can be released into the shallow subsurface from point and line sources that emulate leakage along, for example, abandoned wells or faults [*Lewicki et al.*, 2007]. In July and August 2007, two controlled releases of $CO_2$ were carried out at different rates from a shallow horizontal well; the spatiotemporal evolution of surface leakage signals was characterized by repeated measurements of soil $CO_2$ flux using the accumulation chamber method [*Lewicki et al.*, 2007]. In this study, we deployed an EC station in the field from 8 June 2006 to 4 December 2006 and from 28 May 2007 to 4 September 2007, which allowed us to establish a baseline of background summertime net $CO_2$ flux variability for the study site. To improve our ability to detect $CO_2$ leakage, we apply a filter to the time series that removes the ecological $CO_2$ flux signal that is correlated with changes in intensity of light and soil temperature. Once leakage is detected, we use least squares inversions of measured EC $CO_2$ fluxes and modeled footprint functions to roughly locate and image the geometry of the surface $CO_2$ leak. To our knowledge, this represents the first time that such inversions of EC measurements have been used to model the spatial distribution of heterogeneous surface $CO_2$ fluxes. Our results suggest that under careful, site-specific experiment design, EC is a promising tool to detect and locate leakage signals of moderate to high-magnitude and/or spatial extent, while detection of relatively small leakage signals may require the use of alternative measurement approaches.

## 2. Field Site and $CO_2$ Release Experiments

[5] The $CO_2$ release experiments were conducted at Montana State University, at the Montana Agricultural Experiment Research Center in Bozeman, Montana (45°39′N, 111°04′W). The study site was a ~0.12 $km^2$, nearly flat field, with vegetation composed primarily of prairie grasses, alfalfa, and Canadian thistle. The field was mowed/hayed on 11 July 2006 and then on 22 June 2007. While leaf area index was not measured in this study, it would have been greatly reduced when the field was mowed, thus reducing plant photosynthetic uptake of $CO_2$. A ~0.2- to 1.2-m-thick clay topsoil here overlies an alluvial sandy cobble. A well, oriented 45° to the northeast, was installed in the field using horizontal drilling in December 2006. This well had a 70-m-long perforated and nearly horizontal section at its center and unperforated sections on its two sloping ends (Figure 1). The perforated section was located at ~1.3–2.5 m depth, sub–water table, within the alluvial sandy cobble and was divided into six zones separated by 0.4-m-wide inflatable packers. Five zones were 12 m in length and one zone (on the far southwest end of the well) was 9 m in length. When inflated, the packers prevented fluid flow between the six perforated well zones. Packer inflation and $CO_2$ delivery lines were installed in the well to flow air to the packers and $CO_2$ to each of the six perforated well zones, respectively. Because horizontal drilling was used to install the well, the original soil profile and vegetation over the well were minimally disturbed. From 9 to 18 July 2007, 0.1 t $CO_2$ $d^{-1}$ (100 kg $CO_2$ $d^{-1}$) were released from the well, 13.0 kg $CO_2$ $d^{-1}$ from the far southwest perforated zone and 17.4 kg $CO_2$ $d^{-1}$ from each of the other five zones (hereafter referred to as Release 1). This rate was chosen on the basis of numerical simulations to provide a challenging detection problem while still ensuring that injected $CO_2$ would reach the ground surface. Then, from 3 to 10 August 2007, 0.3 t $CO_2$ $d^{-1}$ (300 kg $CO_2$ $d^{-1}$) were released (hereafter referred to as Release 2). This rate was chosen to obtain a larger surface flux for demonstration purposes. $CO_2$ flow rate to, and pressure within each of the perforated well zones were monitored during the releases.

[6] *Lewicki et al.* [2007] measured soil $CO_2$ flux repeatedly on a daily basis from 7 to 18 July and from 7 to 12 August 2007 using the accumulation chamber method [e.g., *Chiodini et al.*, 1998]. An opaque chamber was used and vegetation within the chamber footprint area was clipped so that only soil $CO_2$ efflux (ecosystem respiration + leakage) was measured. Figure 2 shows contour maps of soil $CO_2$ flux measured prior to Release 1, on day 8 of Release 1, and on day 8 of Release 2. Surface $CO_2$ leakage occurred during both releases at 5–6 points aligned along surface trace of the

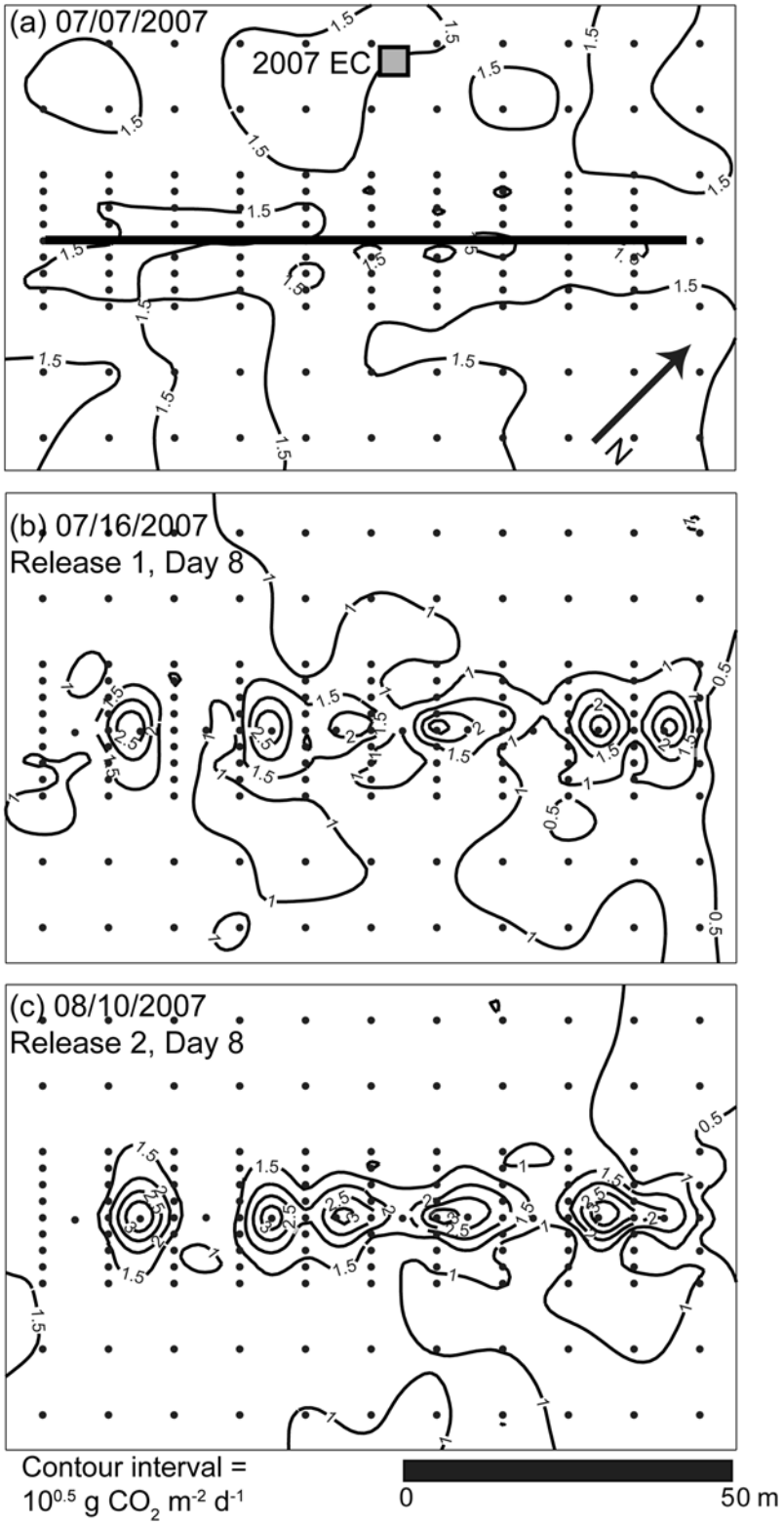


**Figure 2.** Contour maps of log soil $CO_2$ flux for measurements made on (a) 7 July 2007 (background), (b) 16 July 2007 (day 8 of Release 1), and (c) 10 August 2007 (day 8 of Release 2). Dots show measurement locations. Black line and gray square in Figure 2a show approximate locations of surface well trace and 2007 EC station, respectively. The 2006 EC station was located ~60 m north of the 2007 station.

**Table 1.** Slow-Response Subsystem Instrumentation and Measurements

| Instrument | Measured Variable |
|---|---|
| PTB101B barometer (Vaisala, Inc.) | Atmospheric pressure |
| HMP50 humidity and temperature probe (Vaisala, Inc.) | Atmospheric temperature and relative humidity |
| CS800–12 wind set (Climatronics Corp.) | Mean horizontal wind speed and direction |
| CNR-1 radiometer (Kipp & Zonen) | Net radiation |
| LI-200SA pyranometer (LI-COR) | Total insolation |
| LI-190SA quantum sensor (LI-COR) | Photosynthetically active radiation (PAR) |
| TE525 tipping bucket rain gage (Texas Electronics) | Cumulative precipitation |
| ECH2O soil moisture probe (Decagon Devices) | Relative soil moisture profiles |
| Thermocouples (in-house) | Soil temperature profiles |
| HFT3 soil heat flux plates (Radiation and Energy Balance Systems) | Soil heat flux |

well (Figures 2b and 2c). The maximum soil $CO_2$ flux measured during Release 1 was high, $\sim$1600 g $m^{-2}d^{-1}$ ($\sim$420 $\mu$mol $m^{-2}$ $s^{-1}$) relative to background ecosystem respiration fluxes; however, the total $CO_2$ release rate of 0.1 t $d^{-1}$ was of similar magnitude as background ecosystem respiration flux integrated over the relatively small grid area ($7.7 \times 10^3$ $m^2$) [*Lewicki et al.*, 2007]. Leakage fluxes measured during Release 2 along the well trace increased (up to 6000 g $m^{-2}$ $d^{-1}$) relative to Release 1 and the total $CO_2$ release rate of 0.3 t $d^{-1}$ was approximately three times that of background ecosystem respiration flux integrated over the grid area at that time. Further details of soil $CO_2$ flux measurements and the relationship of surface $CO_2$ leakage flux distribution to the well design are given by *Lewicki et al.* [2007].

## 3. Measurement of EC Net $CO_2$ Flux and Environmental Parameters

[7] An EC station was deployed near the center of the field from 8 June to 4 September 2006 and then 27 m northwest of the release well from 28 May to 4 September 2007 (Figure 2a). The location of the station was chosen to take advantage of east-southeasterly prevailing winds, which would frequently situate the EC station downwind of the well leakage source (section 4.1). The station was similar in design to that described by *Billesbach et al.* [2004] and was composed of fast- and slow-response subsystems. The fast-response subsystem included two sensors used to measure the variables necessary to calculate turbulent fluxes of $CO_2$, $H_2O$, heat, and momentum. A Gill-Solent WindMaster Pro sonic three-dimensional anemometer/thermometer (Gill Instruments, Ltd.) measured wind speeds in three orthogonal directions and sonic temperature at 10 Hz. A LI-COR 7500 open-path $CO_2$-$H_2O$ infrared gas analyzer (LI-COR, Inc) measured $CO_2$ and water vapor densities at 10 Hz. Both sensors were mounted atop a tripod tower at 3.2 m height from 8 June to 4 September 2006, 3.0 m height from 28 May to 18 July 2007, and 2.8 m height from 19 July to 4 September 2007.

[8] The slow-response subsystem included sensors (Table 1) associated with a second tripod tower that measured auxiliary meteorological and soil physical parameters. Radiation sensors were mounted to a horizontal bar extending from the tripod tower at 2 m height. Soil moisture profiles (10 and 30 cm depth) were measured at two locations. Since the soil moisture probes were not calibrated for the soil at the study site, we refer to measurements as "relative soil moisture", and only assess the data qualitatively. Soil temperature profiles (10, 20, and 30 cm depth) were measured at two locations. Soil heat flux was measured at four locations at 5 cm depth near the radiometer. Slow-response subsystem variables were measured every 5 s and averaged over 30 min for comparison with turbulent fluxes.

[9] Net $CO_2$ flux ($F_c$) was calculated as the temporal covariance of $CO_2$ density ($c$) and vertical wind velocity ($w$),

$$F_c = \overline{w'c'}, \tag{1}$$

where the overbar denotes time averaging and primes denote fluctuations in $w$ and $c$ relative to their mean values. Fluxes were calculated for 30-min periods. Equation (1) gives the mean vertical turbulent flux of $CO_2$ over a horizontally homogeneous surface under steady state conditions. The lower measurement detection limit is estimated to be 2 g $m^{-2}$ $d^{-1}$ over relatively short vegetation when ecosystem $F_c$ is relatively high. For each half hour of data, the mean lateral ($\overline{v}$) and then the mean vertical ($\overline{w}$) wind velocities were rotated to zero [*Kaimal and Finnigan*, 1994]. The WPL correction for the effects of fluctuation in heat and water vapor on the density of air [*Webb et al.*, 1980] was applied. Raw signals from the infrared gas analyzer and sonic anemometer were evaluated for spikes and all points more than 10 standard deviations (thereby accepting a non-Gaussian tail to the data) away from a 600-s moving average were removed from the data; gaps were then filled using a 10-s moving average. Turbulent fluxes measured during the nighttime under low turbulent conditions can be systematically underestimated [e.g., *Aubinet et al.*, 1999; *Massman and Lee*, 2002]. Auxiliary material Figure S1 shows a plot of $F_c$ versus friction velocity ($u_*$), calculated as the square root of the momentum flux, for nighttime EC measurements made in 2006 and 2007, excluding data collected during Releases 1 and 2, the week following mowing of the field in 2006, and the week following mowing of the field in 2007.[1] We chose two $u_*$ thresholds (0.15 and 0.23 m $s^{-1}$) below which nighttime $F_c$ was discarded in 2006 and 2007 time series to compare their effects on loss of underestimated fluxes. Because nighttime half-hour and average-daily $F_c$ measured in 2006 and 2007 were similar for $u_* > 0.15$ and $u_* > 0.23$ m $s^{-1}$ thresholds (auxiliary material Figure S2) and the 0.15 m $s^{-1}$ threshold allowed us to retain a larger number of data for further analysis and modeling of ecosystem $CO_2$ fluxes

[1] Auxiliary material data sets are available at ftp://ftp.agu.org/apend/jd/2008jd011297. Other auxiliary material files are in the HTML.

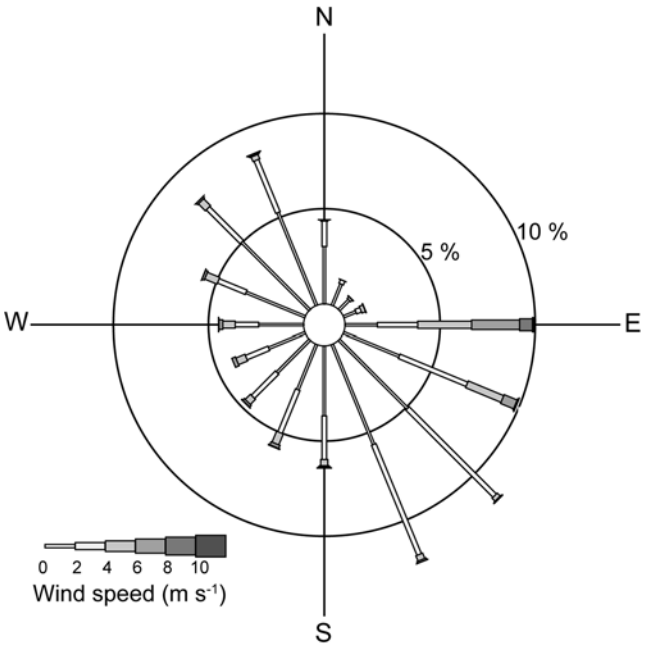


**Figure 3.** Wind rose showing joint frequency distribution of mean horizontal wind speed and direction (half-hour averages) measured in 2006 and 2007.

(section 4.2), we discarded nighttime $F_c$ data corresponding to $u_* \leq 0.15$ m s$^{-1}$. Data were tested for stationarity according to *Foken and Wichura* [1996]. Each 30-min $F_c$ measurement was divided into six 5-min segments. If the difference between the average of the 5-min segments and the 30-min measurement was greater than 30%, then the measurement was considered nonstationary and discarded. On the basis of filtering $F_c$ time series for $u_*$ and stationarity criteria, 43 and 50% of data points were rejected in 2006 and 2007, respectively.

## 4. Results

### 4.1. Meteorology

[10] Winds were primarily either from the east-southeast or from the northwest, with the highest wind speeds measured typically from easterly directions (Figure 3). Figure 4 shows average daily atmospheric temperature, vapor pressure deficit (VPD), PAR, and relative soil moisture and daily cumulative precipitation measured in 2006 and 2007. Average summertime (June–August) atmospheric temperatures were comparable for 2006 and 2007 ($\sim$18°C), with maximum average daily values observed in July (Figures 4a and 4d). Cumulative summertime rainfall was 118.4 mm in 2006; neglecting the week of data loss in July 2007, it was 43.9 mm over the same timeframe in 2007 (Figures 4c and 4f). The highest summertime rainfall occurred in June of 2006 and 2007. In July–August 2007, daily cumulative precipitation exceeded $\sim$1 mm on only 3 days, which occurred either during or several days prior to Releases 1 and 2 (Figure 4f). The rain during Release 2 on 6 August 2007 was associated with a decrease in both atmospheric temperature and VPD. Average daily relative soil moisture showed a long-term decline over the summers of 2006 and 2007, with shorter-term increases observed associated with heavy rain events (Figures 4b and 4e).

### 4.2. Detection of $CO_2$ Leakage Signal Within Ecosystem Variability

[11] The 2006 and 2007 $F_c$ time series are shown in Figure 5. Data gaps were caused by loss of power, intense precipitation events, or filtering with respect to $u_*$ and nonstationarity. On the basis of these data, the field was a net sink for $CO_2$ prior to mowing in both 2006 and 2007. After mowing, the field rapidly became a net source for $CO_2$ when plant leaf area and photosynthetic uptake were dramatically decreased. Daytime $CO_2$ uptake then gradually increased through late July/early August, thereafter remaining relatively constant for the remainder of the 2006 and 2007 observation periods. $CO_2$ leakage during Release 1 was not possible to detect within the large background variability of the $F_c$ time series (Figure 5b). $F_c$ values measured during Release 2 showed a positive shift upward, relative to the weeks prior to and following the release. The mean and standard deviation of the 2006 $F_c$ time series were $-12.4$ and 28.1 g m$^{-2}$ d$^{-1}$, respectively (Figure 6a), whereas the mean and standard deviation of the 2007 $F_c$ time series were $-12.0$ and 28.1 g m$^{-2}$ d$^{-1}$, respectively (Figure 6b).

[12] As observed, the large variability of ecosystem fluxes can mask $CO_2$ leakage signals similar to those studied here, particularly if we lack a priori knowledge of the location of the leakage source. While the location of the leakage source was known in this study, this will not necessarily be the case at many GCS sites where monitoring for potential $CO_2$ leakage is carried out. Consequently, we chose not to filter $F_c$ data for wind direction (i.e., eliminate data corresponding to times when the EC station was located upwind of the well). Estimation and removal of the contribution of net ecosystem exchange (NEE) from the total measured flux, $F_c$ may instead improve our ability to detect leakage at many sites. NEE can be partitioned into photosynthetic uptake by the plant canopy and ecosystem respiration from plants and soil. These constituent fluxes are influenced by a broad range of factors such as meteorology, soil physical and chemical properties, and plant functional and structural characteristics. However, intensity of light and soil temperature are strong drivers of short-time-scale variations in plant photosynthetic uptake and ecosystem respiration, respectively. As a result, empirically derived relationships between these environmental parameters and $F_c$ have been used to decompose $F_c$ into respiration and photosynthetic flux components and gap-fill $F_c$ time series [e.g., *Aubinet et al.*, 1999; *Falge et al.*, 2001; *Reichstein et al.*, 2005; *Fischer et al.*, 2007]. Here, we estimate the ecological $F_c$ signals correlated with changes in light and soil temperature and remove them from the 2006 and 2007 $F_c$ time series.

[13] We use a rectangular hyperbolic function [e.g., *Falge et al.*, 2001] to describe NEE in terms of photosynthetic uptake and respiratory release of $CO_2$,

$$NEE = -\left(\frac{F_{\max}\alpha PAR}{\alpha PAR + F_{\max}}\right) + R_{eco}, \qquad (2)$$

where $F_{max}$ is the maximum $CO_2$ flux at infinite light, $\alpha$ is the apparent quantum yield, and $R_{eco}$ is the respiration $CO_2$

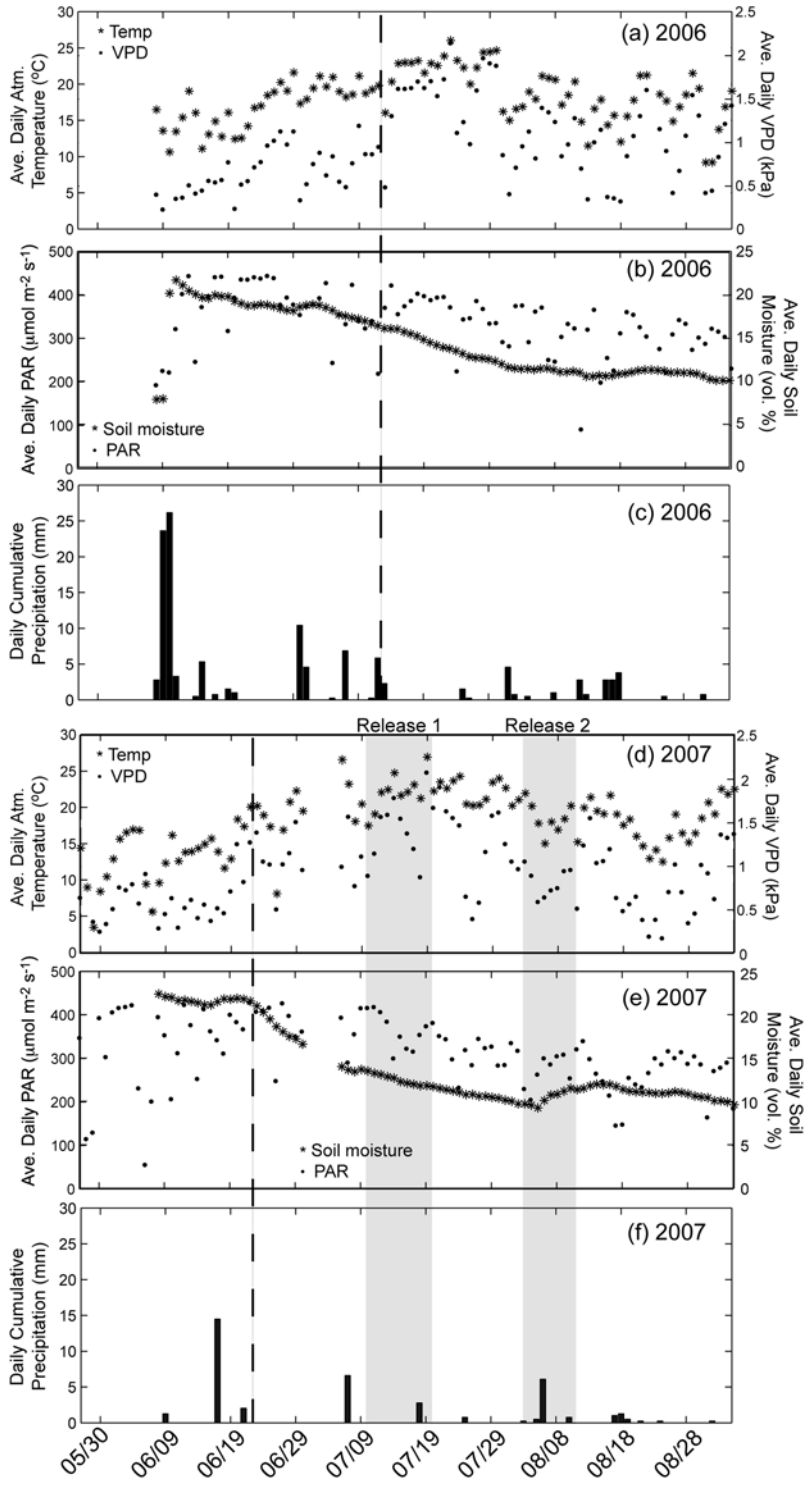


**Figure 4.** Time series of (a) average daily atmospheric temperature (stars) and vapor pressure deficit (VPD; dots), (b) average daily PAR (dots) and relative soil moisture (stars), and (c) daily cumulative precipitation measured in 2006. Time series of (d) average daily atmospheric temperature (stars) and VPD (dots), (e) average daily PAR (dots) and relative soil moisture (stars), and (f) daily cumulative precipitation measured in 2007. Dashed vertical lines show timing of mowing of field. Gray zones show timing of Releases 1 and 2.

flux from plants and soil. Substituting an exponential function that describes the relationship between soil temperature ($T_{soil}$) and $R_{eco}$ [*Lloyd and Taylor*, 1994] into equation (2) yields

$$NEE = -\left(\frac{F_{\max}\alpha PAR}{\alpha PAR + F_{\max}}\right) + b_0 \exp(bT_{soil}), \qquad (3)$$

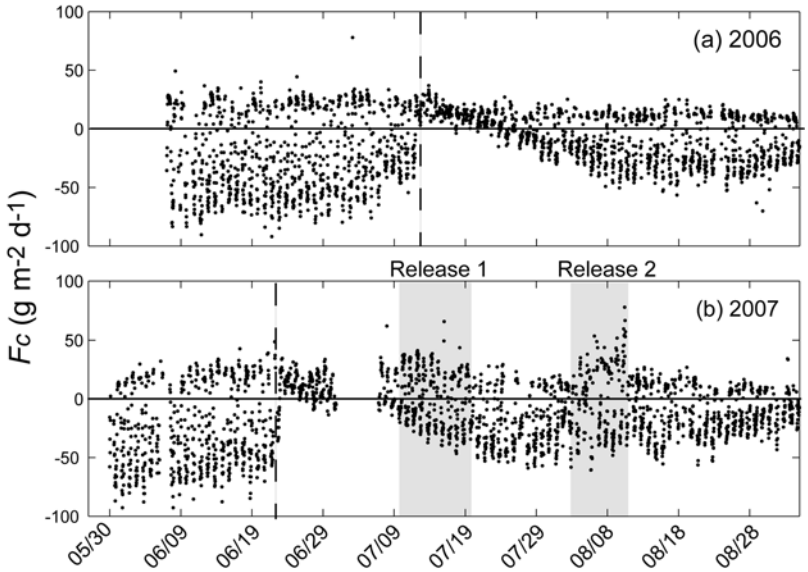


**Figure 5.** Half-hour $F_c$ time series measured in (a) 2006 and (b) 2007. Dashed vertical lines show timing of mowing of the field. Gray zones show timing of Releases 1 and 2.

where $b$ and $b_0$ are empirical coefficients. Using nonlinear optimization methods, equation (3) was fit to half-hour $F_c$, $T_{soil}$ (20 cm depth), and PAR data for 3-day moving (half-hour time step) windows through the entire 2006 and 2007 measurement periods to estimate $\alpha$, $F_{max}$, $b$ and $b_0$ parameters for the center point in the moving window. Predicted values of NEE were then calculated for the center point on the basis of measured $F_c$, $T_{soil}$, and PAR values and best fit parameters. We required a minimum of 20 data points within the 3-day moving window for estimation of $\alpha$, $F_{max}$, $b$ and $b_0$. If fewer data points were present within the window for a given time step, then a gap occurred for predicted NEE. Auxiliary material Figure S3 shows RMS errors as the misfit between predicted NEE and $F_c$ for the 3-day moving windows versus time for 2006 and 2007 time series.

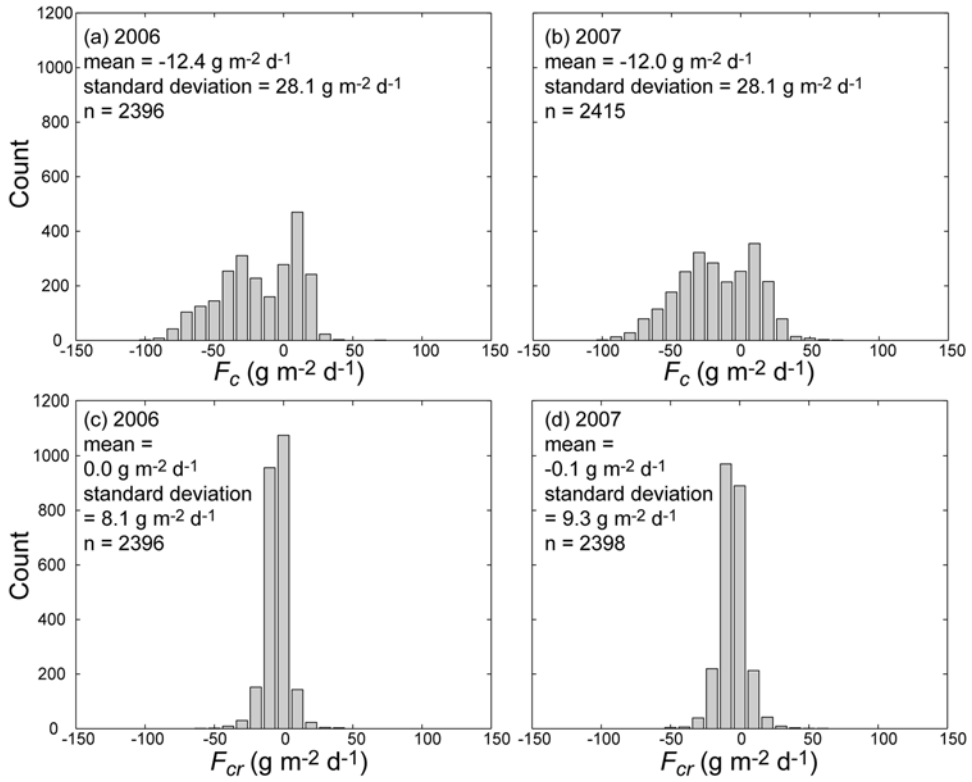


**Figure 6.** Histograms of (a) 2006 $F_c$, (b) 2007 $F_c$, (c) 2006 residual $F_c$ ($F_{cr}$) after ecological flux filter applied, and (d) 2007 $F_{cr}$ after ecological flux filter applied.

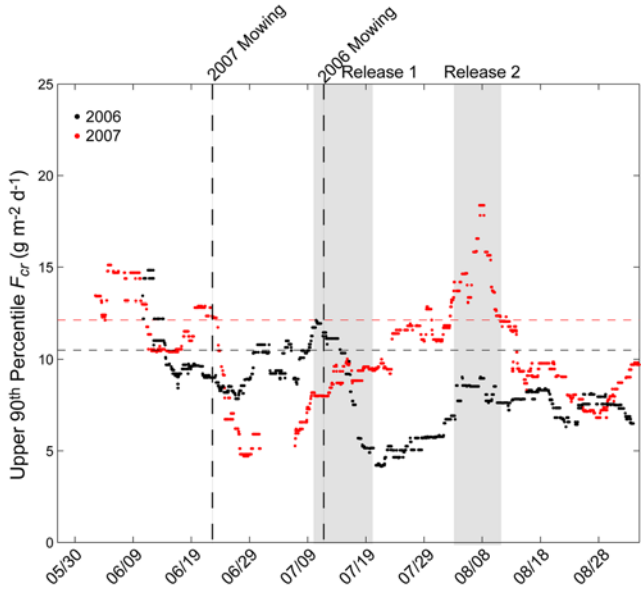


**Figure 7.** Upper 90th percentile residual $F_c$ ($F_{cr}$) for 7-day moving window in 2006 (black dots) and 2007 (red dots). Black and red horizontal dashed lines show 90th percentile residual flux for an exhaustively sampled stationary Gaussian distributions with mean and standard deviation = 0 and 8.1 g $m^{-2}$ $d^{-1}$ (2006), respectively, and 0 and 9.3 g $m^{-2}$ $d^{-1}$ (2007), respectively. Vertical dashed lines show timing of 2006 and 2007 mowing. Gray zones show timing of Releases 1 and 2.

[14] Residual $F_c$ ($F_{cr}$) was calculated by subtracting predicted NEE from measured $F_c$. This simple "ecological flux filter" only reduces fluctuations in $F_c$ that are correlated with variations in $T_{soil}$ and light. The filter does not account for fluctuations in $F_c$ that may be related to variations in, for example, soil moisture, litter, and perhaps even photosynthetic uptake associated with elevated atmospheric $CO_2$ concentrations during a leak. Consequently, $F_{cr}$ values represent our best estimate of fluxes that may result from unmodeled natural processes, background instrument noise, and the $CO_2$ leak of interest. $F_{cr}$ for 2006 and 2007 time series were normally distributed and nearly unbiased (Figures 6c and 6d), with 2006 mean and standard deviation = 0.0 and 8.1 g $m^{-2}$ $d^{-1}$, respectively, and 2007 mean and standard deviation = −0.1 and 9.3 g $m^{-2}$ $d^{-1}$, respectively. Since we expect a $CO_2$ leakage flux signal to be expressed more strongly in the upper tail of a $F_{cr}$ distribution, we isolated the upper 90th percentile $F_{cr}$ to identify points that may be indicative of leakage. A cumulative distribution function of $F_{cr}$ was calculated for a 7-day moving window (advancing in half-hour time steps) and the upper 90th percentile flux of that distribution was assigned to center point of the window. The time series of these upper 90th percentile $F_{cr}$ values for 2006 and 2007 are shown in Figure 7. For a stationary Gaussian distribution, the upper 90th percentile $F_{cr}$ is 1.3 standard deviations above the mean. Assuming stationarity and that the mean is zero for 2006 and 2007 $F_{cr}$ distributions, the upper 90th percentile $F_{cr}$ for these distributions = 10.5 and 12.1 g $m^{-2}$ $d^{-1}$, respectively. These values are shown as the dashed horizontal lines on Figure 7. With the exception of several high-frequency increases in the upper 90th percentile $F_{cr}$ values near the beginning of the 2006 and 2007 observation periods, and the longer-lived, relatively high values observed during Release 2, upper 90th percentile $F_{cr}$ lie close to or below those expected from random sampling a normal distribution. Upper 90th percentile $F_{cr}$ observed near the timing of 2006 and 2007 mowing are close to the 10.5 and 12.1 g $m^{-2}$ $d^{1}$ thresholds, respectively. While upper 90th percentile $F_{cr}$ observed during Release 1 lie within the variability of background values, those measured during Release 2 are highly anomalous and sustained over multiple days (Figure 7).

### 4.3. Location and Quantification of $CO_2$ Leakage Signal

[15] After $CO_2$ leakage was detected during Release 2, we used a radial plot of $F_{cr}$ as a function of mean horizontal wind direction (Figure 8) to determine the direction from which the leakage signal was derived. Figure 8 shows $F_{cr}$ color coded for measurement time, where the relatively large orange dots with black outlines were measured during Release 2. If we assume that $F_{cr} > 18$ g $m^{-2}$ $d^{-1}$ is anomalously high (greater than ~2 standard deviations above the mean), then 19 anomalously high values were measured during Release 2, while 68 were measured during the entire 2007 observation period. Since 28% of anomalously high $F_{cr}$ values were measured during Release 2 and the release only lasted for 8% of the 2007 observation period, anomalously high $F_{cr}$ are more than 3 times overrepresented during Release 2, relative to the rest of the observation period. Anomalously high $F_{cr}$ values were typically measured during Release 2 when the EC station was downwind of the release well (mean horizontal wind direction between 45 and 225°; Figure 8).

[16] The $F_c$ measured by EC at a point ($x_m$, $y_m$, $z_m$) is representative of the weighted average of the upwind surface $CO_2$ emissions. The influence of each surface point source emission on $F_c$ depends on its location relative to the EC sensors. $F_c$ is related to the distribution of source $CO_2$ fluxes ($Q_c$) at the surface ($x'$, $y'$, $z' = z_0$) determined by the footprint or source weight function, $f(x_m - x', y_m - y', z_m - z_0)$ [e.g., *Horst and Weil*, 1992; *Schmid*, 1997],

$$F_c(x_m, y_m, z_m) = \int_{-\infty}^{\infty}\int_{-\infty}^{\infty} Q_c(x', y', z' = z_0) \cdot f(x_m - x', y_m - y', z_m - z_0)\,dx'\,dy'. \quad (4)$$

The footprint function varies with factors such as EC sensor height, atmospheric stability, and surface roughness; however, the value (weight) of the footprint function generally rises to a maximum some distance upwind of the EC sensors, then smoothly falls off in all directions. The total surface influence on $F_c$, or the source area, is the integral beneath the footprint function. Should the spatial distribution of $Q_c$ remain constant over time, changes in $F_c$ will reveal this distribution as the footprint function varies with atmospheric conditions. Thus, in principle, it should be possible to infer the spatial distribution of $Q_c$ using a number of $F_c$ measurements that source different areas, with the purpose of locating and quantifying a potential $CO_2$ leak [e.g., *Miles et al.*, 2005].

[17] We attempt to infer the spatial distribution of surface fluxes during Release 2 using a linear, least squares inversion

[e.g., *Menke*, 1989] of 75 modeled footprint functions and $F_{cr}$ observed during the release. This approach is similar to other geophysical inversions, such as geodetic inferences of fault slip rates based on surface deformations [e.g., *Harris and Segall*, 1987] or tomographic imaging of the seismic velocity structure of the Earth based on multiple travel times of teleseismic waves [e.g., *Dahlen and Tromp*, 1998]. In this particular application, we note that the $F_{cr}$ can be modeled as the weighted sum of the $Q_c$ distribution from which ecological signals have been removed ($Q_{cr}$), hereafter approximated as unvarying in time. Thus, $F_{cr}$ can be written as

$$\overrightarrow{F_{cr}} = \hat{G}\overrightarrow{Q_{cr}}, \tag{5}$$

where $\overrightarrow{F_{cr}}$ is a vector whose length is the number of observations collected during the release, and $\hat{G}$ is a matrix that contains the modeled footprint functions ($f$) that map the unknown surface fluxes ($\overrightarrow{Q_{cr}}$) into $\overrightarrow{F_{cr}}$. Given $\hat{G}$, we estimate the spatial distribution $\overrightarrow{Q_{cr}}$ that best explains the observed $\overrightarrow{F_{cr}}$. We use a least squares solution to this problem, which allows us to write the unknown spatial distribution of surface fluxes in terms of $\overrightarrow{F_{cr}}$ and $\hat{G}$ as follows:

$$\overrightarrow{Q_{cr}} = \left(\hat{G}^T\hat{W}\hat{G}\right)^{-1}\hat{G}^T\hat{W}\overrightarrow{F_{cr}}, \tag{6}$$

where $\hat{W}$ is the covariance matrix of the observed $\overrightarrow{F_{cr}}$, and $\hat{G}^T$ is the transpose of the data kernel. If we assume that fluctuations in $\overrightarrow{F_{cr}}$ are independent from one another, $\hat{W}$ reduces to a diagonal matrix whose dimensions are equal to the number of observations, and whose values are the inverse of the variance of the $\overrightarrow{F_{cr}}$ data ($7.4 \times 10^{-3}$ g$^{-2}$ m$^4$ d$^2$). If many more observations of $\overrightarrow{F_{cr}}$ exist than there are unknown $\overrightarrow{Q_{cr}}$ values, then equation (6) is sufficient to infer the spatial distribution of $\overrightarrow{Q_{cr}}$.

[18] In the current study, there are more $\overrightarrow{Q_{cr}}$ values to be inferred than there are observations of $\overrightarrow{F_{cr}}$. In addition, when equation (6) is applied to, for example, geodetic data, the best fit solutions for $\overrightarrow{Q_{cr}}$ often vary abruptly in space and produce extremely rough solutions that are physically untenable [e.g., *Harris and Segall*, 1987]. For these reasons, following methods developed in the geodetic and seismological communities, we apply an additional constraint to the weighted least squares inversion that requires spatial continuity when finding the best fit values for $\overrightarrow{Q_{cr}}$. This constraint requires the curvature in the values of $\overrightarrow{Q_{cr}}$ to be minimized between adjacent points while satisfying the observed $\overrightarrow{F_{cr}}$ values. This is accomplished by combining $\hat{G}$ with a second $m \times m$ matrix (where $m$ is the number of cells within which $\overrightarrow{Q_{cr}}$ is inferred), hereafter referred to as $\hat{G}_{sm}$. This matrix uses a finite difference expression to calculate curvature on the basis of the inferred flux values at each grid point and those points directly adjacent to it within the inferred source area (assuming points outside of the source area have zero surface flux). In addition, a second vector (referred to as $\overrightarrow{F_{sm}}$) is combined with $\overrightarrow{F_{cr}}$; this vector's length is that of $\overrightarrow{Q_{cr}}$, and its values are set to zero to minimize the curvature of $\overrightarrow{Q_{cr}}$. By combining $\hat{G}$ with $\hat{G}_{sm}$, $\overrightarrow{F_{cr}}$ with $\overrightarrow{F_{sm}}$, and applying equation (6), the values of $\overrightarrow{Q_{cr}}$ will reflect a compromise between the surface flux values inferred from $\overrightarrow{F_{cr}}$ and the requirement of smoothness across the solution space. This has the effect of overly smoothing $\overrightarrow{Q_{cr}}$ in areas that are poorly defined by the observed $\overrightarrow{F_{cr}}$ values, while honoring $\overrightarrow{Q_{cr}}$ in areas well defined by the observed data.

[19] The distribution of $\overrightarrow{Q_{cr}}$ inferred from this method represents a compromise between the constraints provided by observations versus those that require a spatially smooth solution. The relative influence of these two sets of constraints is controlled by specifying the weight that the smoothing function receives in the solution relative to the observations, which we refer to as $w_{sm}$. When $w_{sm}$ is set to a large value, the smoothness of modeled $\overrightarrow{Q_{cr}}$ will be favored over the fit between measured and modeled $\overrightarrow{F_{cr}}$. However, when $w_{sm}$ is set to a small value, the solution will become rougher and more poorly defined for many values of $\overrightarrow{Q_{cr}}$, while the fit between measured and modeled $\overrightarrow{F_{cr}}$ will improve. As is customary in the geophysical literature [e.g., *Harris and Segall*, 1987], for different $w_{sm}$ we plot the misfit between measured and modeled $\overrightarrow{F_{cr}}$ (as the weighted-residual sum of squares; WRSS) versus roughness of $\overrightarrow{Q_{cr}}$,

$$roughness = \sum_{i=1}^{m}\left(Q_{cr,i} - \overline{Q_{cr}}\right)^2. \tag{7}$$

[20] By systematically changing the value of $w_{sm}$, we can determine values of this parameter that result in the greatest decrease in the solution roughness that does not necessitate a correspondingly large change in the data misfit. Thus, we use this plot to identify the optimal $w_{sm}$ that produces a reasonably smooth model result and maintains an acceptable level of misfit.

[21] To model $\overrightarrow{Q_{cr}}$, we discretized the surface surrounding the EC station into an 800 m $\times$ 800 m solution domain. The linear dimension of each square pixel for which $\overrightarrow{Q_{cr}}$ was determined was equal to 10 m. The Flux Source Area Model (FSAM) of *Schmid* [1997], based on analytic solutions of the advection-diffusion equation [*Horst and Weil*, 1992] was used to model footprint functions using the following inputs: (1) $z_m$ = 2.8 m; (2) surface roughness height, $z_0$ = 0.05 m, based on vegetation height measured during Release 2; (3) measured mean horizontal wind direction; (4) cross-wind turbulence near the surface characterized by calculated $\sigma_v/u_*$, where $\sigma_v$ is the standard deviation of the wind speed in the cross-wind direction; and (5) calculated Monin-Obukhov length, $L$ (auxiliary material Data Set S1). We calculated $f$ at the center of each 10 m $\times$ 10 m pixel. Since the source area here was defined as the area from which 90% of the $\overrightarrow{F_{cr}}$ was derived, we renormalized $f$ to reflect this partial sampling by the model. $\overrightarrow{F_{cr}}$ values corresponding to source areas greater than the 0.64 km$^2$ area of the model domain and/or footprint models that did not converge were not considered in the inversion.

[22] Figure 9 shows a plot of the misfit between measured and modeled $\overrightarrow{F_{cr}}$ (WRSS) versus $\overrightarrow{Q_{cr}}$ roughness. A smoothing weight of $10^{-8.5}$ was selected for the model inversion,

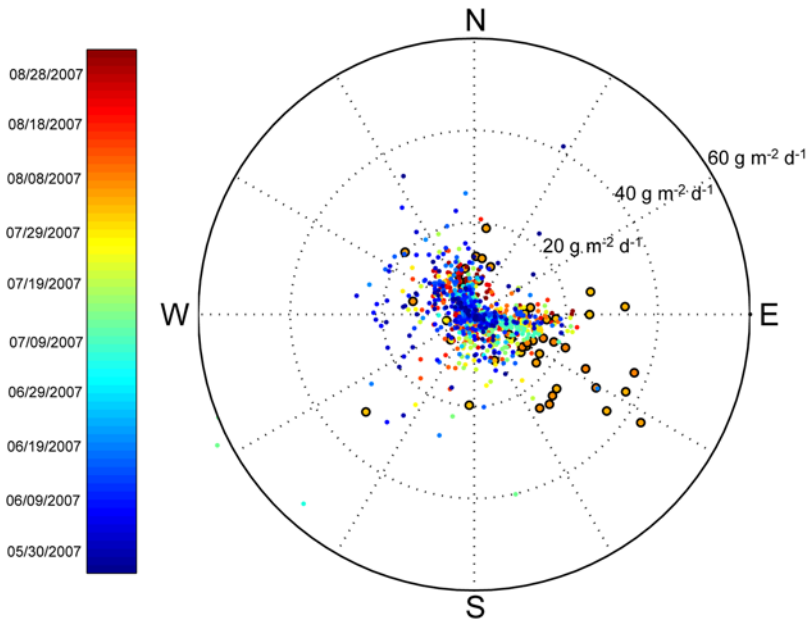


**Figure 8.** Radial plot of $F_{cr}$ as a function of mean horizontal wind direction and time for 2007 data. Color bar denotes timing of measurements. Relatively large orange dots with black outlines are residuals measured during Release 2 (3–10 August 2007).

which provided the optimal compromise between spatial continuity across the model solution space and misfit between measured and modeled $\overrightarrow{F_{cr}}$. Inversion results are shown in Figure 10 for a 400 × 400 m area to highlight the region close to the EC station. Results for the full 800 × 800 m model domain are given in Figure S4. The inversion results show large-scale areas of relatively high $\overrightarrow{Q_{cr}}$ values located at distances greater than ~75 m from, and to the NE and SW of the EC station (Figure 10a). A smaller area of positive $\overrightarrow{Q_{cr}}$ values was modeled closer to and southeast of the EC station. On the basis of the footprint function, only surface fluxes located upwind of the EC station will contribute to $F_{cr}$. Also, surface fluxes located far away from the EC station will tend to contribute a lesser extent to $F_{cr}$ than those located in relatively close proximity. Thus, in minimizing the misfit, the model tends to push extreme flux values into portions of the solution domain for which the EC measurements provide little constraint. We constructed a contour map of the sum of footprint weights based on the 75 modeled footprint functions (Figure 10b), the "footprint climatology" [e.g., *Amiro*, 1998; *Göckede et al.*, 2008]. This map highlights those portions of the solution space that were well

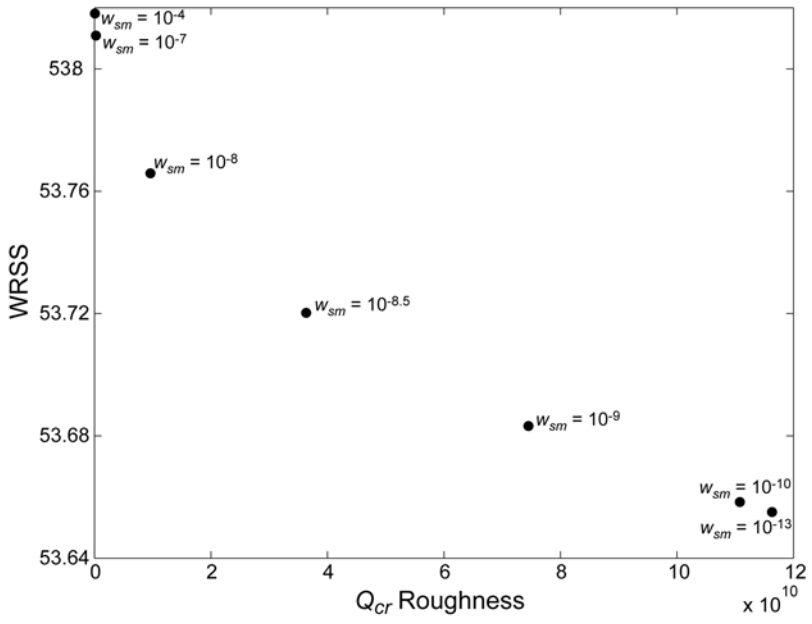


**Figure 9.** Plot of misfit between measured and modeled $\overrightarrow{F_{cr}}$ (as weighted-residual sum of squares; WRSS) versus $\overrightarrow{Q_{cr}}$ roughness for different $w_{sm}$. A $w_{sm} = 10^{-8.5}$ was used in inversion.

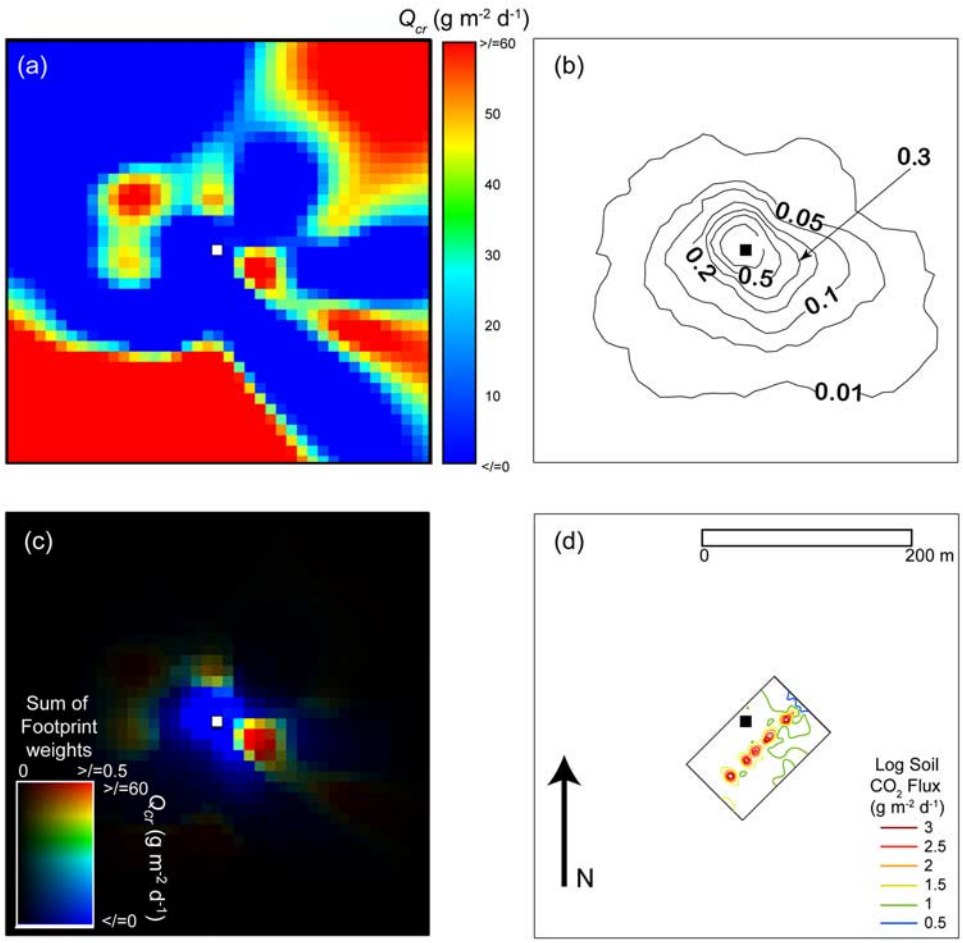


**Figure 10.** Maps of (a) modeled surface $CO_2$ flux ($\overrightarrow{Q_{cr}}$) (note scale on color bar, where $Q_{cr} \geq 60$ and $\leq 0$ g m$^{-2}$ d$^{-1}$ are dark red and blue, respectively), (b) footprint climatology (contour map of sum of footprint weights based on 75 inverted footprint functions), and (c) modeled surface $CO_2$ flux shaded for uncertainty based on sum of footprint weights (Figure 10b), where degree of masking increases with uncertainty. (d) Contour map color-coded for log soil $CO_2$ flux measured during Release 2 on 10 August 2007 (Figure 2c). White or black squares indicate location of EC station.

defined by the EC measurements and provides a qualitative assessment of the relative uncertainty of the model inversion results. Surface areas located within ~50 m of the EC station were weighted most highly in modeled footprint functions; $\overrightarrow{Q_{cr}}$ values modeled within those regions were therefore well defined by EC measurements and associated with the greatest certainty. Surface fluxes located greater than ~ 75 m from the EC station were poorly resolved by EC measurements; smoothing thus dominates inversion results in these regions. Figure 10c shows the map of modeled $\overrightarrow{Q_{cr}}$ values, shaded for relative uncertainty so that $\overrightarrow{Q_{cr}}$ values that are not resolved by observations are masked. An area of relatively high $\overrightarrow{Q_{cr}}$ is located within ~30 m and southeast of the EC station. While the shape of this region is less elongate than the surface $CO_2$ flux leakage signal measured during Release 2 (Figure 10d), its location relative to the EC station is similar. Importantly, the central portion of the linear surface $CO_2$ flux leakage signal in Figure 10d is located in an area of greater footprint weight (Figure 10b) than the two ends of the signal. For comparison, Figure S4 shows maps of $\overrightarrow{Q_{cr}}$, modeled using $w_{sm}$ values of $10^{-13}$, $10^{-8.5}$, and $10^{-4}$. The area of relatively high $\overrightarrow{Q_{cr}}$ located within ~30 m and southeast of the EC station is consistent for all three inversions, while those areas defined only by smoothing vary strongly with $w_{sm}$.

[23] To test our ability to quantify the surface leakage rate associated with Release 2 on the basis of modeled $\overrightarrow{Q_{cr}}$, we integrated $\overrightarrow{Q_{cr}}$ values over the area of the accumulation chamber measurement grid (Figures 2 and 10d), which yielded $CO_2$ discharge = 0.02 t d$^{-1}$. On the basis of accumulation chamber measurements, *Lewicki et al.* [2007] estimated a leakage $CO_2$ discharge on day 8 of Release 2 = 0.33 t d$^{-1}$. Assuming that the surface leakage $CO_2$ discharge was equal to the $CO_2$ release rate during Release 2 (0.3 t d$^{-1}$), accumulation chamber measurements recorded 110% of the surface leakage rate, while EC measurements, based on modeled $\overrightarrow{Q_{cr}}$, recorded 7% of the surface leakage rate.

## 5. Discussion and Conclusions

[24] The $CO_2$ release rates of Releases 1 and 2 and their associated surface leakage signals provided a challenge for detection of $CO_2$ leakage by EC. For example, the surface $CO_2$ leakage rate measured using the accumulation chamber

method during Release 1 was less than or similar to the background ecosystem respiration flux integrated over the relatively small measurement grid area [*Lewicki et al.*, 2007]. Also, both releases resulted in surface $CO_2$ flux leakage signals of small spatial extent, relative to the EC flux source areas.

[25] Measurements of $F_c$ made during Summer 2006 and prior to Release 1 in 2007 allowed us to establish a baseline of background summertime variability for the study site.

[26] We first examined the raw 2007 $F_c$ time series (Figure 5b) to assess whether $CO_2$ leakage signals associated with Releases 1 and 2 were possible to detect. No convincing change in $F_c$ was discernable during the timeframe of Release 1, whereas a positive shift upward in $F_c$ was detectable during Release 2, relative to the week prior to and those following the release.

[27] Removal of the ecosystem signal from the $F_c$ time series that was correlated with changes in PAR and soil temperature greatly improved our ability to detect $CO_2$ leakage during Release 2. Application of this ecological flux filter reduced the variability of and removed the negative bias from the 2006 and 2007 $F_{cr}$ distributions, relative to the corresponding $F_c$ distributions (Figure 6). Plotting the upper 90th percentile $F_{cr}$ versus time (Figure 8) allowed us to isolate anomalously high residual fluxes associated with $CO_2$ leakage during Release 2. The 90th percentile $F_{cr}$ values expected assuming stationary Gaussian distributions for 2006 and 2007 were similar (10.5 and 12.1 g $m^{-2}$ $d^{-1}$, respectively), suggesting that similar factors controlled variability of the residuals during both years. These factors likely include the influence of fluctuations in VPD, precipitation, and soil moisture on $F_c$, other unmodeled natural processes, and to a lesser extent, EC instrument noise. Since the 2006 and 2007 $F_{cr}$ distributions were not truly stationary, we observed variations in the upper 90th percentile $F_{cr}$ away from the expected values. For example, the high-frequency spikes in these values that occurred at the beginning of the 2006 and 2007 measurement periods are likely related to measurement noise during heavy precipitation events. Finally, while the $CO_2$ leakage signal associated with Release 2 emerged clearly in Figure 7, $CO_2$ leakage during Release 1 remained undetectable after the ecological $F_c$ signal was removed. Detection of relatively small $CO_2$ leakage signals by EC will likely be difficult at many sites. However, if we are able to model and remove $F_c$ signals associated with additional natural processes and instrument noise, detection ability may be improved.

[28] Once a $CO_2$ leakage signal has been detected, EC may assist in its location and quantification when used in concert with other surface $CO_2$ flux measurement techniques. For example, we constructed a radial plot of $F_{cr}$ as a function of wind direction (Figure 8), which confirmed that anomalously high $F_{cr}$ values were measured during Release 2 typically when the EC station was downwind of the well leakage source. Without a priori knowledge of the leakage source location, such a radial plot could be used to estimate the direction from which $CO_2$ leakage is derived. EC footprint modeling would determine the approximate source areas from within which directionally consistent anomalously high $F_{cr}$ values originate. A point $CO_2$ flux measurement approach such as the accumulation chamber method could then be used to locate and quantify $CO_2$ leakage [e.g., *Lewicki et al.*, 2007] within those areas.

[29] Alternatively, EC has the potential to locate and quantify $CO_2$ leakage signals when used alone if (1) multiple EC stations are deployed in different locations or an array of EC sensors is installed at more than one height at a given location and simultaneously sample a leakage area with different flux footprints or (2) a leakage area is relatively stable over time and is sampled repeatedly by a single EC station with varying flux footprints. We showed that it was possible to locate a leakage signal with a location, geometry, and magnitude such as that of Release 2 using a single EC station by inversion of 75 $F_{cr}$ measurements and corresponding footprint functions (Figure 10). To our knowledge, this is the first study to invert EC measurements to infer the spatial distribution of heterogeneous surface fluxes. Importantly, however, our map of modeled $\vec{Q}_{cr}$ only roughly resolved the location and geometry of the leakage signal, while the leakage rate was underestimated by ~93%. Overall, the ability to locate, map the geometry of, and quantify a given $CO_2$ leakage signal using EC will be very challenging and depend on a wide range of factors, such as location of the EC sensors, magnitude, geometry, and spatiotemporal stability of the signal, atmospheric conditions at the time of the measurements, surface roughness, site topography, and the number of EC measurements available for the inversion. Also, relatively high and heterogeneous $CO_2$ leakage emissions could potentially cause advection, leading to underestimation of the leakage signal by EC. In our case, the limited number of EC measurements available for inversion during the relatively short timeframe of Release 2 strongly impacted the resolution of modeled $\vec{Q}_{cr}$; a greater number of measurements would presumably improve the results. Furthermore, we showed that on the basis of factors such as EC sensor location, site surface roughness, and atmospheric conditions, only the area within ~75 m of the EC station contributed substantially to $F_c$ measurements (Figure 10b). Since the $CO_2$ leakage source was situated within this region, we were able to detect and locate it. In particular, the central part of the linear surface $CO_2$ flux leakage signal (Figure 10d) was located within an area of high footprint weight, relative to the two ends of the signal. This likely led to the anomalously high modeled $\vec{Q}_{cr}$ within a point-source region (Figure 10c) near the center of the measured signal in Figure 10d, and could have contributed to our underestimation of total leakage discharge based on $\vec{Q}_{cr}$. Given the challenges associated with the use of EC to detect, locate, and quantify $CO_2$ leakage signals of small magnitude and/or spatial extent within a background ecosystem, the application of EC in GCS monitoring programs should be guided by detailed site characterization, careful EC experiment design, and, ideally, the use of complementary measurement techniques.

[30] **Acknowledgments.** We are grateful to five anonymous reviewers whose scrutiny and constructive comments greatly improved this paper. We thank J. Ajo-Franklin for careful review of the draft manuscript, K. Gullickson for assistance in the field, and H.P. Schmid for the FSAM source code. This work was funded by the ZERT Project, Assistant Secretary for Fossil Energy, Office of Sequestration, Hydrogen, and Clean Coal Fuels, NETL, of the U.S. Department of Energy under contract DE-AC02-05CH11231.

## References

Amiro, B. D. (1998), Footprint climatologies for evapotranspiration in a boreal catchment, *Agric. For. Meteorol.*, *90*, 195–201, doi:10.1016/S0168-1923(97)00096-8.

Anderson, D. E., and C. D. Farrar (2001), Eddy covariance measurement of $CO_2$ flux to the atmosphere from an area of high volcanogenic emissions, Mammoth Mountain, California, *Chem. Geol.*, *177*, 31–42, doi:10.1016/S0009-2541(00)00380-6.

Aubinet, M., et al. (1999), Estimates of the annual net carbon and water exchange of European forests: The EUROFLUX methodology, *Adv. Ecol. Res.*, *30*, 113–175, doi:10.1016/S0065-2504(08)60018-5.

Baldocchi, D. D. (2003), Assessing the eddy covariance technique for evaluating carbon dioxide exchange rates of ecosystems: Past, present, and future, *Global Change Biol.*, *9*, 479–492, doi:10.1046/j.1365-2486.2003.00629.x.

Billesbach, D. P., M. L. Fischer, M. S. Torn, and J. A. Berry (2004), A portable eddy covariance system for the measurement of ecosystem-atmosphere exchange of $CO_2$, water vapor, and energy, *J. Atmos. Oceanic Technol.*, *21*, 639–650, doi:10.1175/1520-0426(2004)021<0639:APECSF>2.0.CO;2.

Chiodini, G., G. R. Cioni, M. Guidi, B. Raco, and L. Marini (1998), Soil $CO_2$ flux measurements in volcanic and geothermal areas, *Appl. Geochem.*, *13*, 543–552, doi:10.1016/S0883-2927(97)00076-0.

Cortis, A., C. M. Oldenburg, and S. M. Benson (2008), The role of optimality in characterizing $CO_2$ seepage from geologic carbon sequestration sites, *Int. J. Greenhouse Gas Control*, *2*, 640–652, doi:10.1016/j.ijggc.2008.04.008.

Dahlen, F. A., and J. Tromp (1998), *Theoretical Global Seismology*, Princeton Univ. Press, Princeton, N. J.

Falge, E., et al. (2001), Gap filling strategies for defensible annual sums of net ecosystems exchange, *Agric. For. Meteorol.*, *107*, 43–69, doi:10.1016/S0168-1923(00)00225-2.

Fischer, M. L., D. P. Billesbach, J. A. Berry, R. J. Riley, and M. S. Torn (2007), Spatiotemporal variations in growing season exchanges of $CO_2$, $H_2O$, and sensible heat in agricultural fields of the southern Great Plains, *Earth Interact.*, *11*, 1–21, doi:10.1175/EI231.1.

Foken, T., and M. Y. Leclerc (2004), Methods and limitations in validation of footprint models, *Agric. For. Meteorol.*, *127*, 223–234, doi:10.1016/j.agrformet.2004.07.015.

Foken, T., and B. Wichura (1996), Tools for quality assessment of surface-based flux measurements, *Agric. For. Meteorol.*, *78*, 83–105, doi:10.1016/0168-1923(95)02248-1.

Göckede, M., et al. (2008), Quality control of CarboEurope flux data–Part 1: Footprint analyses with flux data quality assessment to evaluate sites in forest ecosystems, *Biogeosciences*, *5*, 433–450.

Harris, R., and P. Segall (1987), Detection of a locked zone at depth on the Parkfield, California segment of the San Andreas fault, *J. Geophys. Res.*, *92*, 7945–7962, doi:10.1029/JB092iB08p07945.

Horst, T. W., and J. C. Weil (1992), Footprint estimation for scalar flux measurements in the atmospheric surface-layer, *Boundary Layer Meteorol.*, *59*, 279–296, doi:10.1007/BF00119817.

Intergovernmental Panel on Climate Change (2005), *IPCC Special Report on Carbon Dioxide Capture and Storage*, Cambridge Univ. Press, Cambridge, U. K.

International Energy Agency (1997), Carbon dioxide utilization, report, IEA Greenhouse Gas R and D Programme, Paris.

International Energy Agency (2004), Prospects for $CO_2$ capture and storage, report, 252 pp., IEA Publ., Paris.

Kaimal, J. C., and J. J. Finnigan (1994), *Atmospheric Boundary Layer Flows: Their Structure and Measurement*, Oxford Univ. Press, Oxford, U. K.

Leuning, R., D. Etheridge, A. Luhar, and B. Dunse (2008), Atmospheric monitoring and verification technologies for $CO_2$ geosequestration, *Int. J. Greenhouse Gas Control*, *2*, 401–404, doi:10.1016/j.ijggc.2008.01.002.

Lewicki, J. L., G. E. Hilley, and C. M. Oldenburg (2005), An improved strategy to detect $CO_2$ leakage for verification of geologic carbon sequestration, *Geophys. Res. Lett.*, *32*, L19403, doi:10.1029/2005GL024281.

Lewicki, J. L., C. M. Oldenburg, L. Dobeck, and L. Spangler (2007), Surface $CO_2$ leakage during two shallow subsurface $CO_2$ releases, *Geophys. Res. Lett.*, *34*, L24402, doi:10.1029/2007GL032047.

Lewicki, J. L., M. L. Fischer, and G. E. Hilley (2008), Six-week time series of eddy covariance $CO_2$ flux at Mammoth Mountain, California: Performance evaluation and role of meteorological forcing, *J. Volcanol. Geotherm. Res.*, *171*, 178–190, doi:10.1016/j.jvolgeores.2007.11.029.

Lloyd, J., and J. A. Taylor (1994), On the temperature-dependence of soil respiration, *Funct. Ecol.*, *8*, 315–323, doi:10.2307/2389824.

Massman, W. J., and X. Lee (2002), Eddy covariance flux corrections and uncertainties in long-term studies of carbon and energy exchanges, *Agric. For. Meteorol.*, *113*, 121–144, doi:10.1016/S0168-1923(02)00105-3.

Menke, W. (1989), *Geophysical Data Analysis: Discrete Inverse Theory*, Academic Press, San Diego, Calif.

Miles, N., K. Davis, and J. Wyngaard (2005), Detecting leaks from $CO_2$ reservoirs using micrometeorological methods, in *Geologic Storage of Carbon Dioxide With Monitoring and Verification*, vol. 2, *Carbon Dioxide Capture for Storage in Deep Geologic Formations-Results From the $CO_2$ Capture Project*, edited by S. M. Benson, pp. 1031–1044, Elsevier, London.

Oldenburg, C. M., J. L. Lewicki, and R. P. Hepple (2003), Near-surface monitoring strategies for carbon dioxide storage verification, *Rep. LBNL-54089*, 54 pp., Lawrence Berkeley Nat. Lab., Berkeley, Calif.

Reichstein, M., et al. (2005), On the separation of net ecosystem exchange into assimilation and ecosystem respiration: Review and improved algorithm, *Global Change Biol.*, *11*, 1424–1439, doi:10.1111/j.1365-2486.2005.001002.x.

Schmid, H. P. (1997), Experimental design for flux measurements: Matching scales of observations and fluxes, *Agric. For. Meteorol.*, *87*, 179–200, doi:10.1016/S0168-1923(97)00011-7.

Webb, E. K., G. I. Pearman, and R. Leuning (1980), Correction of flux measurements for density effects due to heat and water vapour transfer, *Q. J. R. Meteorol. Soc.*, *106*, 85–100, doi:10.1002/qj.49710644707.

Werner, C., J. C. Wyngaard, and S. L. Brantley (2000), Eddy-correlation measurement of hydrothermal gases, *Geophys. Res. Lett.*, *27*, 2925–2928, doi:10.1029/2000GL011765.

Werner, C., G. Chiodini, D. Voigt, S. Caliro, R. Avino, M. Russo, T. Brombach, J. Wyngaard, and S. Brantley (2003), Monitoring volcanic hazard using eddy covariance at Solfatara volcano, Naples, Italy, *Earth Planet. Sci. Lett.*, *210*, 561–577, doi:10.1016/S0012-821X (03)00127-4.

L. Dobeck and L. Spangler, Department of Chemistry and Biochemistry, Montana State University, 108 Gaines Hall, PO Box 173400, Bozeman, MT 59717, USA.

M. L. Fischer, Environmental Energy Technology Division, Lawrence Berkeley National Laboratory, 1 Cyclotron Road, Berkeley, CA 94720, USA.

G. E. Hilley, Department of Geological and Environmental Sciences, Stanford University, Stanford, CA 94305, USA.

J. L. Lewicki, C. M. Oldenburg, and L. Pan, Earth Sciences Division, Lawrence Berkeley National Laboratory, 1 Cyclotron Road, Berkeley, CA 94720, USA. (jllewicki@lbl.gov)